Tetrahedral Clustering in Molten Lithium under Pressure

Isaac Tamblyn,[1] Jean-Yves Raty,[2] and Stanimir A. Bonev[1,*]
[1]Department of Physics, Dalhousie University, Halifax, Nova Scotia, B3H 3J5, Canada
[2]FNRS-University of Liege, Sart-Tilman 4000, Belgium
(Received 18 May 2008; revised manuscript received 20 June 2008; published 14 August 2008)

A series of electronic and structural transitions are predicted in molten lithium from first principles. A new phase with tetrahedral local order characteristic of sp^3 bonded materials and poor electrical conductivity is found at pressures above 150 GPa and temperatures as high as 1000 K. Despite the lack of covalent bonding, weakly bound tetrahedral clusters with finite lifetimes are predicted to exist. The stabilization of this phase in lithium involves a unique mechanism of strong electron localization in interstitial regions and interactions among core electrons. The calculations provide evidence for anomalous melting above 20 GPa, with a melting temperature decreasing below 300 K, and point towards the existence of novel low-symmetry crystalline phases.

DOI: 10.1103/PhysRevLett.101.075703 PACS numbers: 64.70.dj, 61.20.Ja, 62.50.−p, 71.22.+i

At ambient pressure (P) and temperature (T), Li can be regarded as the prototype for an ideal metal. However, theoretical studies [1] have predicted that as a result of increased core-valence electron interactions, low-T dense solid Li would undergo a series of symmetry-breaking transitions, culminating in a Li_2-paired crystal with semimetallic properties at pressures above 150 GPa. Besides the regular transition at 7.5 GPa from bcc to fcc structure [2], measurements to date [3] have confirmed only an initial transition at 39 GPa from fcc to a less compact structure with a 16-atom cubic cell ($cI16$ space group) via an intermediate disordered phase ($hR1$). The existence and properties of even lower-coordinated structures at higher pressures remains an open question due to the lack of experimental data and difficulties associated with conclusive theoretical predictions of low-temperature thermodynamic crystalline stability.

It was shown recently [4] that solid-solid transitions in Na are preceded by analogous changes in its liquid at much lower pressures. Similar behavior was also suggested for other light alkalis. This raises the intriguing question, answered in this Letter, of whether the existence of low-symmetry structures in Li [1,3,5–8] could be established by investigating its molten phase. In addition to being remarkable in itself, finding low-coordinated structures in simulations of a liquid would constitute rather conclusive evidence for the existence of solid phases with similar local order under comparable compression.

We have carried out first principles molecular dynamics (FPMD) simulation of liquid Li in the density range corresponding to $3.06 > r_s > 1.60$ [where $\frac{4}{3}\pi(r_s a_0)^3 = V/N$, a_0 is the Bohr radius, V the volume, and N the number of valence electrons] at temperatures up to 3000 K, and of the known crystalline phases: bcc, fcc, and $cI16$, between 0 and 90 GPa. Density functional theory with a plane wave basis set and the Born-Oppenheimer approximation were used for all simulations [9]. They were performed in the NVT ensemble with cubic supercells and periodic boundary conditions. For the bcc and $cI16$ solids, and all liquids we used 128 atom supercells with Γ-point sampling of the Brillouin zone. Simulations of the fcc solids were performed with 108 atoms and a denser 8 $\mathbf{k}$-point grid, which was necessary in order to obtain the correct electronic structure and crystalline stability in this smaller cell. Most simulations ran for at least 10 ps, with some up to 20 ps, while for obtaining the melting temperatures we have computations as long as 200 ps. Convergence tests were carried out for all controlled approximations as well as the validity of the pseudopotential approximation [12]. Good agreement was obtained with existing liquid experimental data [13].

Results for the structural analysis of the liquid along the 1000 K isotherm are presented in Fig. 1. Initially, the first peak of the pair correlation function, $g(r)$, broadens [Fig. 1(a)] in a way previously observed in Na [4]. Upon further compression, it splits entirely, indicating significant further lowering in the coordination. Several distinct regions with different liquid structures can be identified [see Fig. 1(b)], which correlate well with the electronic and melting properties discussed further below: (i) $r_s \gtrsim 2.60$ ($P < 23$ GPa); (ii) $2.60 \gtrsim r_s \gtrsim 2.05$ (23 GPa $< P <$ 150 GPa); and (iii) $r_s \lesssim 2.05$ ($P > 150$ GPa). The initial changes are analogous to those observed in liquid Na [4]—a transition from a bcc-like to an fcc-like local order in (i), followed in (ii) by lowering in the coordination [number of neighbors under the symmetrized first peak of $g(r)$] to $8 + 4 + \ldots$, and the liquid acquiring a $cI16$-like local order.

In (iii), the density-rescaled average distances to neighbors 1–4 continue to contract even faster, while the next eight, as well as 13–16, move away. As a result, by $r_s = 1.80$ ($P \sim 370$ GPa), the first coordination shell completely splits in two, the coordination becomes only four and remains roughly so up to at least $r_s = 1.6$ ($P \sim 810$ GPa). The distribution of angles among the nearest

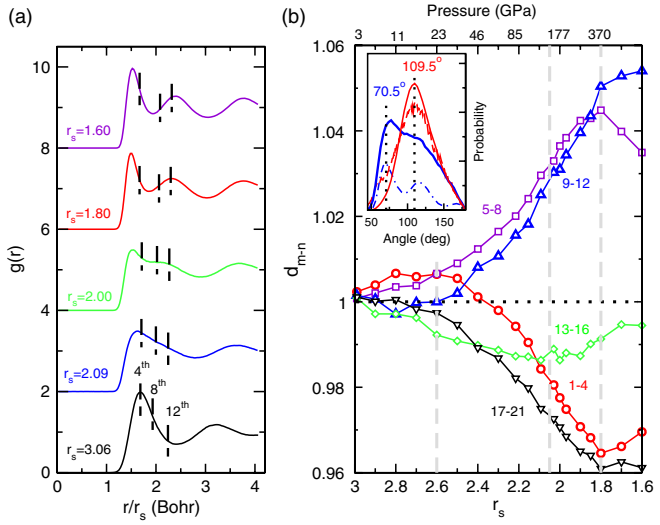

FIG. 1 (color online). Structural changes in molten Li along the 1000 K isotherm. (a) Pair correlation function $g(r)$. Vertical dashed lines indicate the average positions of the 4th, 8th, and 12th neighbors. (b) First, average interatomic distances are computed to the first (r_1), second (r_2), and so on, neighbors. Next, density-rescaled distances are calculated as $d_i = (r_i/r_s)/(r_i^0/r_s^0)$, where $r_s^0 = 3.06$ and r_i^0 refers to distances obtained at r_s^0. Finally, d_{m-n} is the averaged value of d_i for neighbors, i, from m to n (see curve labels). The inset shows bond angle distributions between the first two neighbors in molten Li (solid curves) for $r_s = 3.06$ (blue or dark gray) and 1.80 (red or gray), of solid bcc Li (dashed blue or dark gray line) at 500 K and $r_s = 3.06$, and of molten diamond [24] around 250 GPa (dashed red or gray curve). Angles among nearest neighbors in ideal bcc (70.50°) and diamond (109.50°) crystals are indicated. The bcc data are scaled by a factor of 1/3 for clarity.

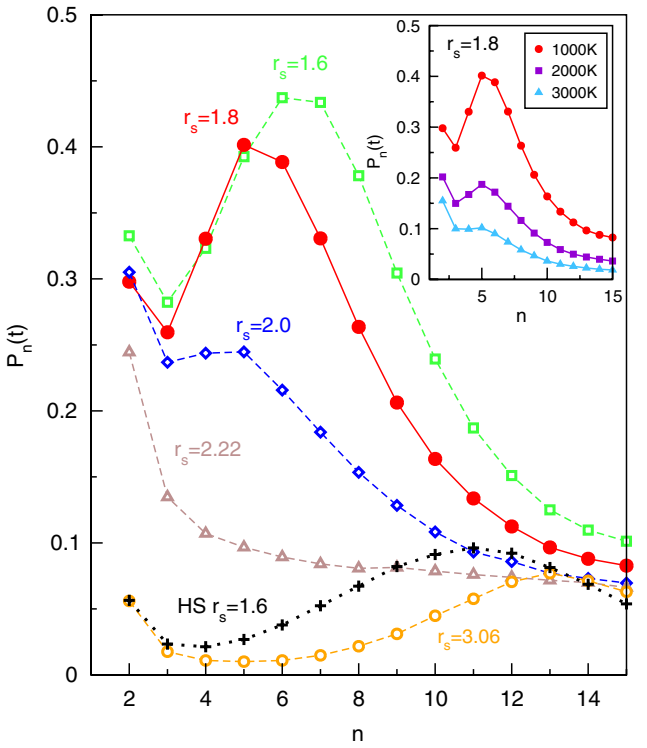

FIG. 2 (color online). Survival probability $P_n(t)$ of clusters as a function of their size n. Results are shown for Li and for a hard-sphere (HS) liquid. The times at which the $P_n(t)$'s are evaluated are: 43 fs (for $r_s = 3.06$), 27 fs ($r_s = 2.22$), 20 fs ($r_s = 2.00$), 15 fs ($r_s = 1.80$) and 12 fs ($r_s = 1.60$) for Li, and 20 fs for the HS liquid. The HS radius is chosen such that the self-diffusion constant and the short-distance $g(r)$'s of the HS and Li liquids are roughly the same. Computations with HS's at lower densities show rapidly decreasing values of $P_n(t)$, already an order of magnitude lower at $r_s = 2.0$. The inset shows $P_n(t)$ of Li clusters as a function of temperature at $r_s = 1.80$.

neighbors also becomes rather unexpected [inset in Fig. 1(b)] as it has a peak at 109.5°. The parallel with the liquids of materials with sp^3 bonding is indeed striking when compared with the corresponding angle distribution in molten carbon, obtained by melting diamond at similar pressure [inset in Fig. 1(b)]. Therefore, there is a large pressure range, 150 GPa $< P <$ 810 GPa, for which we predict that Li has tetrahedral local order, hitherto not seen in a liquid metal, but characteristic of semiconductor liquids with sp^3 bonding.

The apparent structural similarity with covalently bonded liquids has prompted us to investigate the persistence probability of Li clusters. For this purpose, we evaluate a function $P_n(t)$, which gives the statistical probability for the first $(n-1)$ nearest neighbors found around an atom at time t to be the same as those found at time $t = 0$. For completely uncorrelated particles, $P_n(t)$ would drop monotonically with increasing n for any fixed t. As shown in Fig. 2, $P_n(t)$ changes qualitatively when density is increased. The appearance of a peak at $n = 5$ is evidence for a weak metastability of the tetrahedral clusters. To estimate the importance of caging effects, we have also carried out simulations of hard-sphere liquids. The comparison with Li (Fig. 2) demonstrates that the peak in $P_n(t)$ of Li is much higher, indicating significantly stronger interatomic correlations.

We now examine the changes in the electronic properties that are likely to drive the structural transitions. With increasing density, the DOS at the Fermi level gradually decreases [Fig. 3(a)]. A similar effect, interpreted as a Peierls symmetry breaking, was observed in liquid Na [4], except that its strength in Li is stronger, which can be understood in terms of an increasing hardness of the effective repulsive potential. To interpret these changes and their likely consequences, we first look at the valence electron bandwidth [Fig. 3(b)]. It increases with increasing density, as expected upon densification. This tendency remains up to $P \sim 23$ GPa ($r_s = 2.6$), which matches well the pressure range over which the liquid becomes more compact. Above this pressure, the bandwidth begins to decrease due to a development of partial (p-character) bonding, which lowers the band-structure energy. The DOS develops a marked peak well below the Fermi level. This is also the range over which the coordination in the liquid begins to decrease. Finally, starting at $P \sim 150$ GPa

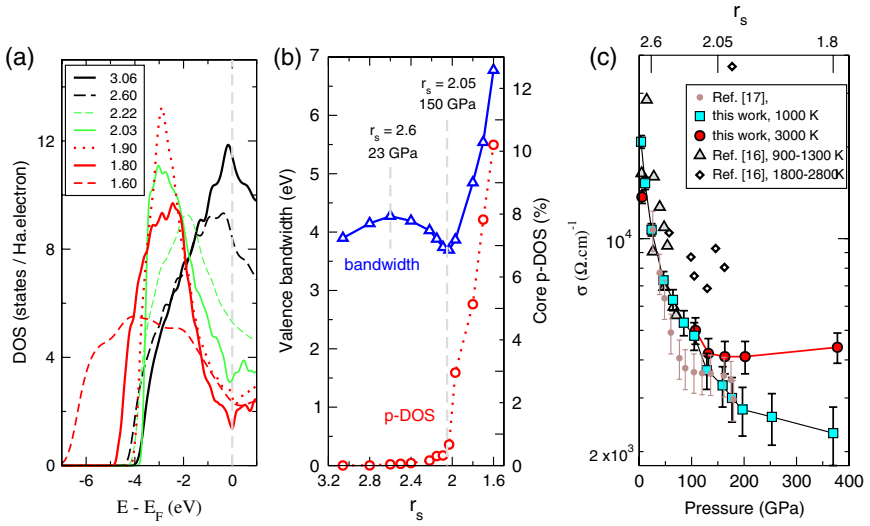

FIG. 3 (color online). Electronic properties. (a) Density of states, DOS. The corresponding r_s values are listed in the legend. (b) Valence electron bandwidth (blue or dark gray triangles) and integrated DOS of core electrons with p angular momentum character, p-DOS (red or gray circles). (c) Calculated and measured [16,17] dc conductivity, σ.

($r_s < 2.05$), the valence band begins to broaden again, but the DOS at the Fermi level does not decrease much further. This density range coincides with the conditions under which the tetrahedral coordination develops. For $r_s < 2.05$ ($P > 150$ GPa) the p angular momentum character of the *core* electrons increases rapidly [Fig. 3(b)], indicating core-core overlap. The volume available to the valence electrons, now squeezed into interstitial regions, decreases linearly with increasing density and hence the rapid increase of the valence bandwidth. The resulting "antidiamond" structure (inset in Fig. 4) is with ions forming a tetrahedral network, but the valence electrons occupying preferentially the voids of the diamond structure instead of being located between adjacent ions.

The electrical conductivity (σ) of compressed liquid Li exhibits exactly the opposite P and T dependence usual for metals. Our computations [14] show that along the 1000 K isotherm it has nearly a tenfold drop between 3 and 150 GPa. When heating the liquid to 3000 K near and above 250 GPa, there is about twofold increase in σ, but this increase vanishes at lower P. These results are compared with measurements [16,17] for which we now provide an explanation that is very different from what was originally proposed.

First, the electron localization and decrease of DOS at the Fermi level lead to a significant drop in σ with P. Second, the above-mentioned electronic changes are closely related to structural transitions from a higher to a lower-coordinated liquid. This trend is reversed when heating the liquid at a constant V; it reverts to a more homogeneous local order as favored by entropy. The result is an increase of σ with T above 150 GPa. This effect is of course countered by increased electron-ion scattering at high T. At $P \sim 100$ GPa, the two effects cancel, and at lower P where the structural changes are less significant, the scattering effects dominate. This explanation for the observed changes in σ is different from what was previously suggested and we emphasize that the increase in conductivity observed at the highest-P measurements by Fortov *et al.* [16] is not a pressure but a temperature effect. Despite the fact that the latter data were obtained using a model equation of state to estimate the density, resistivity, and T, the general trend of increased σ with T at sufficiently high P is consistent with our findings.

Finally, we compute the melting curve (Fig. 4) using a heat-until-melting approach, which provides an upper

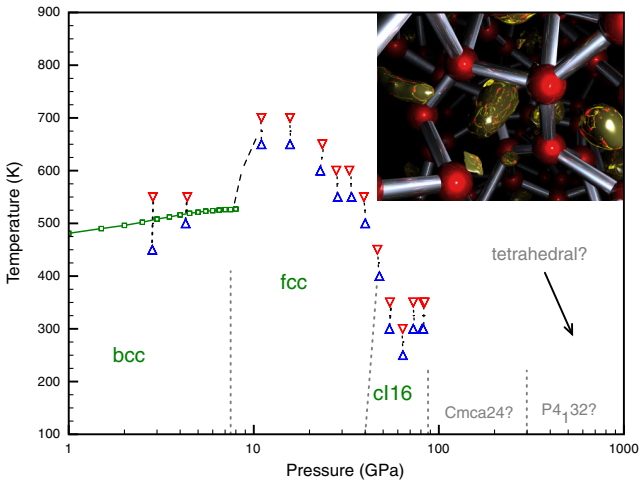

FIG. 4 (color online). Melting curve of Li. Experimental data [25,26] are shown as open squares. Up-triangle and down-triangle pairs indicate FPMD simulations of solid and liquids phases, respectively, on the same isochore, which bracket the melting temperature. The dashed line connecting the highest-pressure experimental data to the theoretical points near 10 GPa is only a guide to the eye. The vertical dotted lines indicate ambient temperature solid phase boundaries, except for the phase line between fcc and $cI16$ which is estimated based on their respective melting temperatures. Here $Cmca24$ and $P4_132$ are the crystalline structures previously proposed [7,8] for $P >$ 90 GPa at 0 K. The inset shows the tetrahedral structure which develops in the liquid ($T = 1000$ K) above 150 GPa. The ions are shown as red (or gray) balls, each connected to its nearest neighbors. Isosurfaces of the valence charge density are shown as reflective (gold) surfaces.

bound for the melting temperatures (T_m). The method was shown [4] to be valid for Na for reasons that are likely to hold for Li. The melting curve has a steep negative slope between roughly 20 and 80 GPa, with T_m dropping from (680 ± 25) K to (275 ± 25) K. The shape of the melting curve above bcc is relatively flat, which is consistent with a gradual transformation in the liquid from bcc-like to fcc-like local order. The fcc solid is denser than bcc and the melting slope above it initially increases, in accordance with the Clapeyron equation. The onset of symmetry-breaking transitions lead to lowering of the liquid electronic band-structure energy, its densification, and, hence, to the turnover of the melting curve above the fcc phase. The maximum T_m is near 20 GPa-exactly where we identified the onset of the changes towards lower coordination. The anomalous melting behavior persists until pressures where the solid also begins to undergo Peierls symmetry-breaking transitions.

The crystalline structures above 70 GPa are yet to be measured experimentally. Previous suggestions include *Cmca* [1] and *Cmca*24 [7]. More recently, application of an evolutionary algorithm [8] has predicted $P4_132$ above 300 GPa. Our findings here suggest that crystalline phases with tetrahedral local order should be energetically competitive. Dynamical effects may play a significant role in their stabilization. The appearance of such a phase, and especially its persistence at high T, is completely unexpected. While the modifications in Li are initially driven by Peierls-like distortions, at higher P they are determined by core-core electron interactions and valence electron localization (resulting from core-valence interactions). This behavior describes a distinct regime, likely present in other materials, where both valence and core electrons are responsible for chemical and physical properties. Such effects could have far reaching consequences in areas ranging from planetary modeling to the study of superconductivity under pressure [18–21]. Another interesting aspect is the implications these results have for comparisons between the alkalis and dense hydrogen. It has been discussed [1,22] that similarities between Li and H could be used to predict high-pressure phases, including superconductivity [23], in metallic H. However, as shown here, the properties of Li at extreme pressures are strongly determined by interactions among core electrons, which are not present in H.

Work supported by NSERC, CFI, and the Killam Trusts. Computational resources provided by ACEnet, IRM, WestGrid, SHARCNET, and LLNL. We thank E. Schwegler, R. Redmer, A. Correa, M. Bastea, and V. E. Fortov for discussions.

*stanimir.bonev@dal.ca

[1] J. B. Neaton and N. W. Ashcroft, Nature (London) **400**, 141 (1999).
[2] B. Olinger and W. Shaner, Science **219**, 1071 (1983).
[3] M. Hanfland *et al.*, Nature (London) **408**, 174 (2000).
[4] J. Y. Raty, E. Schwegler, and S. A. Bonev, Nature (London) **449**, 448 (2007).
[5] G. J. Ackland and I. R. McLeod, New J. Phys. **6**, 138 (2004).
[6] N. E. Christensen and D. L. Novikov, J. Phys. Condens. Matter **14**, 10879 (2002).
[7] R. Rousseau *et al.*, Chem. Phys. Chem. **6**, 1703 (2005).
[8] Y. Ma, A. R. Oganov, and Yu. Xie, Phys. Rev. B **78**, 014102 (2008).
[9] The FPMD simulations were performed with the Perdew, Burke, and Ernzerhof generalized gradient approximation (PBE-GGA) using PWSCF [10] with Troullier Martins 1-electron pseudopotentials for some melting simulations at $P < 50$ GPa and VASP [11] with all-electron PAW for the rest.
[10] S. Baroni *et al.* (http://www.pwscf.org).
[11] G. Kresse and J. Hafner, Phys. Rev. B **47**, 558 (1993).
[12] FPMD tests were carried out with 8 **k**-points, with 256 atom cells, large plane wave cutoff (up to 25 Ha), and time steps as small as 16 a.u. (1 a.u. = 0.02419 fs). The validity of our PAW potential at the highest densities considered was tested on isolated Li_5 tetrahedral clusters by comparing with all-electron DFT-GGA (both PBE and B3LYP) and CCSD(T) calculations produced with the Gaussian quantum chemistry code, using a $-3/r$ ion potential.
[13] L. E. Gonzalez, D. J. Gonzalez, and M. Canales, Z. Phys. B **100**, 601 (1996), and references therein.
[14] DOS and σ (using Kubo-Greenwood) were computed with ABINIT [15] using an all-electron PAW pseudopotential, PBE-GGA, and 32 **k**-points (tests were made with up to 1000 **k**-points and independently with VASP).
[15] X. Gonze *et al.*, Comput. Mater. Sci. **25**, 478 (2002).
[16] V. E. Fortov *et al.*, JETP Lett. **74**, 418 (2001).
[17] M. Bastea and S. Bastea, Phys. Rev. B **65**, 193104 (2002).
[18] N. W. Ashcrof, Nature (London) **419**, 569 (2002).
[19] K. Shimizu *et al.*, Nature (London) **419**, 597 (2002).
[20] V. V. Struzhkin *et al.*, Science **298**, 1213 (2002).
[21] S. Deemyad and J. S. Schilling, Phys. Rev. Lett. **91**, 167001 (2003).
[22] R. M. Martin, Nature (London) **400**, 117 (1999).
[23] N. W. Ashcroft, Phys. Rev. Lett. **21**, 1748 (1968).
[24] A. Correa, S. A. Bonev, and G. Galli, Proc. Natl. Acad. Sci. U.S.A. **103**, 1204 (2006).
[25] H. Luedemann and C. Kennedy, J. Geophys. Res. **73**, 2795 (1968).
[26] R. Boehler, Phys. Rev. B **27**, 6754 (1983).